

Shimmering Darkness: Mapping the Evolution of Supernova-Neutrino-Boosted Dark Matter within the Milky Way

Yen-Hsun Lin^{1,*} and Meng-Ru Wu^{1,2,3,†}

¹*Institute of Physics, Academia Sinica, Taipei 115, Taiwan*

²*Institute of Astronomy and Astrophysics, Academia Sinica, Taipei 106, Taiwan*

³*Physics Division, National Center for Theoretical Sciences, Taipei 106, Taiwan*

Supernova-neutrino-boosted dark matter (SN ν BDM) has emerged as a promising portal for probing sub-GeV dark matter. In this work, we investigate the behavior of BDM signatures originating from core-collapse supernovae (CCSNe) within the Milky Way (MW) over the past one hundred thousand years, examining both their temporal evolution and present-day spatial distributions. We show that while the MW BDM signature is approximately diffuse in the nonrelativistic regime, it exhibits significant temporal variation and spatial localization when the BDM is relativistic. Importantly, we compare these local MW signatures with the previously proposed diffuse SN ν BDM (DBDM), which arises from the accumulated flux of all past SNe in the Universe [1]. In the nonrelativistic limit, DBDM consistently dominates over the local diffuse MW BDM signature. Only when the MW BDM becomes ultrarelativistic and transitions into a transient, highly-localized signal, it can potentially surpass the DBDM background. This work thus reinforces the importance of DBDM for SN ν BDM searches until the next galactic SN offers new opportunities.

I. INTRODUCTION

Although strong evidence suggests that dark matter (DM) is both abundant and stable in our Universe, its fundamental nature, whether particle-like or wave-like, remains elusive. Over the past decades, numerous DM candidates have been proposed, ranging from ultra-light axion-like particles [2] to weakly interacting massive particles (WIMPs) [3]. These theoretical developments have been accompanied by a variety of experimental search strategies, including direct detection [4–10], indirect searches [11–17], and collider-based approaches [18, 19]. While stringent constraints have been placed on WIMPs with masses m_χ above the GeV scale, the sub-GeV regime remains challenging due to the associated low recoil signals. Despite these difficulties, an increasing number of novel detection schemes have emerged, leveraging new materials such as superconductors, quantum devices, and other mechanisms [20–60]. Innovative uses of neutrino detectors, exploiting dark counts [61] and solar reflection [62] are also proposed.

Recently, scenarios where DM is upscattered by high-energy cosmic particles have attracted growing interest. Such boosted dark matter (BDM) offers a promising avenue to probe sub-GeV DM in large underground neutrino and DM experiments [1, 63–102] such as Super-Kamiokande (SK) [103], Hyper-Kamiokande (HK) [104], DUNE [105], and JUNO [106], due to the sufficient energy deposition and flux required to achieve plausible detection significance within a reasonable exposure time.

Among various BDM scenarios, supernova-neutrino-boosted dark matter (SN ν BDM) [1, 89, 98, 102] offers a unique way for possible extraction of m_χ by utilizing

the temporal profile of BDM flux that arrived after the detection of SN ν when the next galactic core-collapse SN (CCSN) takes places [89, 98]. Besides individual CCSN, the accumulated SN ν BDM flux from all past supernovae (SNe) throughout cosmic history contributes to a diffuse BDM (DBDM) component [1]. This component is analogous to the well-known diffuse SN ν background [107, 108], and can be readily explored by current and upcoming neutrino and DM experiments before the next galactic CCSN occurs.

While above works mainly focus on the SN ν BDM whose kinetic energy $T_\chi \gtrsim \mathcal{O}(\text{MeV})$, comparable to the energy scale of SN ν , Ref. [102] recently discussed the SN ν BDM flux from past CCSNe in the Milky Way (MW) for $T_\chi \lesssim \mathcal{O}(\text{MeV})$ and its relevance to semiconductor-based DM experiments. One key assumption taken in Ref. [102] is to approximate this component as completely time-independent when the typical SN ν BDM duration (t_{van}) from a single CCSN is longer than the average time interval between two successive CCSNe in MW, τ_{CCSN} , by taking a time-averaged SN ν spectrum across the MW as the boosting source. In this work, we aim to fully address this assumption by examining the full temporal and spatial dependence of SN ν BDM in the MW across a wide range of m_χ/T_χ . By performing Monte Carlo (MC) simulation to generate the locations and ages of $\sim 1,600$ CCSNe in the MW over the past one hundred thousand years, we compute the fine-resolved spatial distribution at present time and the temporal evolution of SN ν BDM flux over a span of $\sim 1,000$ yrs by summing over the contribution from all CCSNe. Our results quantify that the all-sky, temporal flux of the MW SN ν BDM varies by a factor of $\lesssim 5$ when $m_\chi/T_\chi \gtrsim \mathcal{O}(0.1)$, which corresponds to $t_{\text{van}} \gtrsim \mathcal{O}(800)$ yrs $\gtrsim 13\tau_{\text{CCSN}}$ ¹. For $t_{\text{van}} \simeq \tau_{\text{CCSN}}$,

* yensun@phys.ncku.edu.tw

† mwu@as.edu.tw

¹ We note that a similar requirement has been recently suggested

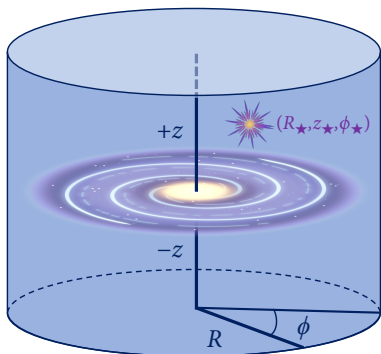


FIG. 1. Schematic plot for the coordinate system used to generate the mock SN dataset in this work. GC is located at the origin of the cylindrical coordinate system, where (R, z, ϕ) correspond to the radial distance, vertical height, and azimuthal angle, respectively. The coordinates (R_*, z_*, ϕ_*) indicate the position of a SN.

the all-sky $\text{SN}\nu$ BDM flux still varies substantially over time and cannot be approximated by the averaged flux. Similarly, the contribution from individual CCSNe to the present-day angular distribution of $\text{SN}\nu$ BDM largely overlap only for $m_\chi/T_\chi \gtrsim \mathcal{O}(0.1)$ and can be considered as diffuse. For $t_{\text{van}} \lesssim \tau_{\text{CCSN}}$, $\text{SN}\nu$ BDM from different CCSNe can in principle be separated if good angular resolution in experiments can be provided. In addition, we find that the diffuse $\text{SN}\nu$ BDM flux from past CCSNe in MW computed here is generally smaller than the DBDM flux for $m_\chi/T_\chi \gtrsim \mathcal{O}(0.01)$ by a factor of a few, suggesting that DBDM remains the dominant component for diffuse $\text{SN}\nu$ BDM searches.

The structure of this paper is as follows. In Sec. II, we describe the MC simulation of CCSN distributions in the MW over the past 100,000 years. A brief overview of $\text{SN}\nu$ BDM physics are provided in Sec. III for completeness. Numerical results illustrating the temporal and spatial distributions of BDM are presented in Sec. IV and are compared to the DBDM flux. In addition, given that hundreds of supernova remnants (SNRs) have been observed, we also performed a parallel analysis using this realistic dataset in Sec. V and discuss the implication. We summarize our findings in Sec. VI.

All calculations presented in this study were performed using our python package `snorer` [110]. A comprehensive user manual is also provided [111].

II. SAMPLING SUPERNOVA DISTRIBUTION IN MILKY WAY

To compute the $\text{SN}\nu$ BDM flux contribution from past CCSNe in the MW, we generate a set of data that records

	Σ_0 ($M_\odot \text{ kpc}^{-2}$)	R_d (kpc)	z_d (kpc)
thin	8.96×10^8	2.5	0.3
thick	1.83×10^8	3.02	0.9

TABLE I. Parameter values describing the density distribution of the stellar disc components in MW.

the time and location of each CCSN over the past 10^5 yrs with the following procedure. We take the CCSN rate $R_{\text{CCSN}} = 1/\tau_{\text{CCSN}} \approx 1.63$ per century [112] and assume a uniform probability distribution function in time. For the location, we assume a spatial distribution following the stellar density profile of the MW. We take the cylindrically symmetric MW stellar density profiles of the bulge and disc components, ρ_b and ρ_d , respectively from Ref. [113]:

$$\rho_b(R, z) = \frac{\rho_{0,b}}{[1 + r'(R, z)/r_0]^\alpha} \exp\left[-\frac{r'^2(R, z)}{r_{\text{cut}}^2}\right], \quad (1)$$

and

$$\rho_d(R, z) = \frac{\Sigma_0}{2z_d} \exp\left(-\frac{|z|}{z_d} - \frac{R}{R_d}\right). \quad (2)$$

Here, R and z denote the cylindrical radial and vertical coordinates relative to the Galactic Center (GC) (see Fig. 1). For the bulge, $r' = \sqrt{R^2 + (z/q)^2}$, with parameters $\alpha = 1.8$, $r_0 = 0.075$ kpc, $r_{\text{cut}} = 2.1$ kpc, $q = 0.5$, and $\rho_{0,b} = 9.93 \times 10^{10} M_\odot \text{ kpc}^{-3}$. For the disc, we further distinguish between thin and thick components, ρ_d^{thin} and ρ_d^{thick} , using parameters listed in Table I in Eq. (2) respectively.

The normalized spatial probability distribution function for SNe, p_{SN} , is given by

$$p_{\text{SN}}(R, z) = \mathcal{N}R[\rho_b(R, z) + \rho_d^{\text{thin}}(R, z) + \rho_d^{\text{thick}}(R, z)], \quad (3)$$

where the normalization constant \mathcal{N} satisfies

$$2\pi \int_0^{R_{\text{max}}} dR \int_{-z_{\text{max}}}^{z_{\text{max}}} dz p_{\text{SN}}(R, z) = 1. \quad (4)$$

Since ρ_b and ρ_d rapidly fall off exponentially beyond $(R, z) \sim (40, 5)$ kpc, we take $(R_{\text{max}}, z_{\text{max}}) = (50, 10)$ kpc in Eq. (4).

Given the above temporal and spatial distributions, we use the python MC sampling package `emcee` [114] to obtain the times and locations of 1,667 CCSNe in our dataset spanning over a time duration in $0 \leq t \leq 10^5$ yrs, where $t = 10^5$ yr denotes the present time. As we focus exclusively on CCSNe, we refer these events as SNe throughout the rest of the paper for simplicity.

Fig. 2 shows the spatial locations (blue dots) of these 1,667 SNe in our sample projected on the x - y plane, where $x = R \cos \phi$ and $y = R \sin \phi$. Also shown is the location of the Earth, chosen to be on the $-x$ axis with coordinate $(R, z, \phi) = (R_e, 0, -\pi)$ or $(x, y, z) = (-R_e, 0, 0)$. $R_e = 8.5$ kpc is the distance between Earth and GC. The

for estimating the amount of “diffuse $\text{SN}\nu$ component” due to $\text{SN}\nu$ deflected by heavy DM with $m_\chi \gtrsim \mathcal{O}(1)$ GeV in MW [109].

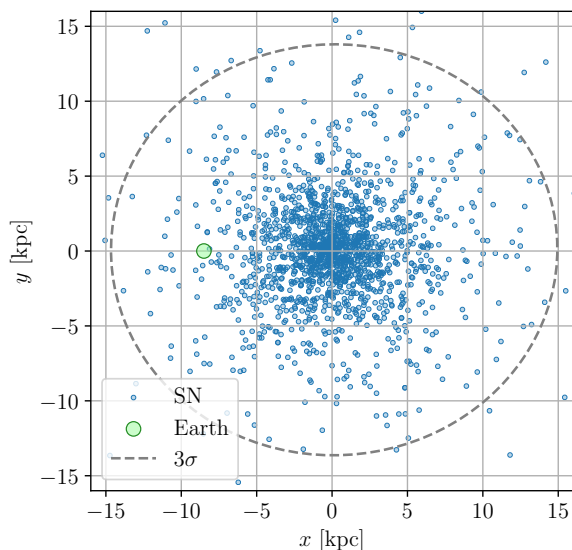


FIG. 2. Locations of SNe (blue dots) over the past 100,000 years across MW projected on the x - y plane. The Earth, shown as a green circle, is located at $(x, y, z) = (-R_e, 0, 0)$ in Cartesian coordinates. The gray dashed line encloses the 3σ range of SN occurrence probability. A total of 1,667 SNe are included in this dataset.

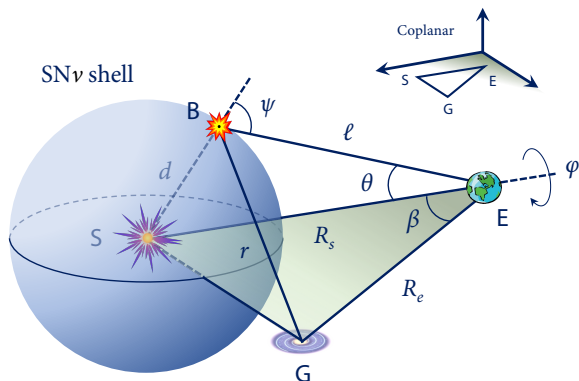


FIG. 3. Schematic plot showing the geometry and coordinates used to compute the SN ν BDM. SN (S), GC (G), and Earth (E) lie on the same plane. Halo DM is upscattered by SN ν at location B on the outward-propagating SN ν shell.

gray dashed contour in Fig. 2 encloses the 3σ probability range. Although the projected plot does not show the distribution in z , we take that into account in our calculation. For the age of each SN, it is given by

$$t_{\text{age}} = 10^5 \text{ yrs} - t_{\text{SN}}, \quad (5)$$

where t_{SN} is the occurring time of the SN.

III. SN ν BDM IN MILKY WAY

In this section, We review the basic framework of SN ν BDM [1, 89, 98] and extend the discussion on the signal duration of SN ν BDM from a single SN, t_{van} , to cover the nonrelativistic limit with $m_\chi/T_\chi \gg 1$. Throughout this work, we adopt the assumption of an energy-independent DM- ν cross section for demonstration, noting that the same framework can be applied to any generic and energy-dependent particle models predicting DM-visible sector interactions [115–130] as done in Ref. [98].

To compute the SN ν BDM flux at Earth, we take a different coordinate system shown in Fig. 3 where Earth (E) is located at the origin. We use R_s (R_e) to denote the distance between SN at S (GC at G) and Earth at E. DM can be boosted by at any location B on the expanding spherical shell of SN ν whose radius with respect to the SN location is d . The resulting BDM that arrives at Earth needs to travel a distance ℓ along the direction defined by the scattering angle ψ . The angle θ denotes the viewing angle at Earth relative to the direction of the SN. It is important to note that $n_\chi(r)$, which is assumed to follow the NFW profile [131, 132], is not azimuthally symmetric in φ unless the SN lies along the \overline{GE} axis so that the angle $\beta = 0$; see App. B in Ref. [98] for detailed discussions. With the geometry specified above, the associated temporal profile and the angular distribution (viewed from Earth) of SN ν BDM flux can be evaluated unambiguously.

A. BDM flux at Earth

The BDM emissivity at B is given by [98]

$$j_\chi(r, d, T_\chi, \psi) = cn_\chi(r) \left(\frac{1}{2\pi} \frac{d\sigma_{\chi\nu}}{d \cos \psi} \right) \frac{dn_\nu}{dE_\nu} \left(\frac{dE_\nu}{dT_\chi} \frac{v_\chi}{c} \right), \quad (6)$$

where E_ν is the neutrino energy, c the speed of light, and T_χ the kinetic energy transferred to DM, expressed as

$$T_\chi = \frac{E_\nu^2}{E_\nu + m_\chi/2} \left(\frac{1 + \cos \theta_c}{2} \right), \quad (7)$$

with $\theta_c = 2 \tan^{-1}(\gamma \tan \psi)$ the scattering angle in the center-of-mass frame of scattering and $\gamma = (E_\nu + m_\chi)/\sqrt{m_\chi(2E_\nu + m_\chi)}$. The BDM velocity $v_\chi/c = \sqrt{T_\chi(2m_\chi + T_\chi)/(m_\chi + T_\chi)}$. The differential DM- ν cross section (assumed to be uniform in the center-of-mass frame) take the form

$$\frac{1}{2\pi} \frac{d\sigma_{\chi\nu}}{d \cos \psi} = \sigma_0 g_\chi(\psi), \quad (8)$$

where

$$g_\chi(\psi) = \frac{\gamma^2 \sec^3 \psi}{\pi(1 + \gamma^2 \tan^2 \psi)^2} \quad (9)$$

is the lab-frame angular distribution at B for scattering angle $\psi \in [0, \pi/2]$ [89]. In the following discussion, we fix $\sigma_0 = 10^{-35} \text{ cm}^2$ for demonstration.

For the SN ν number density at B, we take

$$\frac{dn_\nu}{dE_\nu} = \sum_i \frac{L_{\nu_i}}{4\pi d^2 \langle E_{\nu_i} \rangle c} E_\nu^2 f_{\nu_i}(E_\nu), \quad (10)$$

where $L_{\nu_i} = L_{\nu, \text{tot}}/6 \approx 5 \times 10^{51} \text{ erg s}^{-1}$ is the luminosity of each flavor (ν_e , ν_μ , ν_τ , and their antiparti-

cles). The average energies are taken as $\langle E_{\nu_e} \rangle = 11 \text{ MeV}$, $\langle E_{\bar{\nu}_e} \rangle = 16 \text{ MeV}$, and $\langle E_{\nu_x} \rangle = 25 \text{ MeV}$, with $\nu_x \in \{\nu_\mu, \nu_\tau, \bar{\nu}_\mu, \bar{\nu}_\tau\}$. The function f_{ν_i} is the Fermi-Dirac distribution with pinch parameter $\eta_{\nu_i} \equiv \mu_{\nu_i}/T_{\nu_i} = 3$, such that $T_{\nu_i} \approx \langle E_{\nu_i} \rangle/3.99$. All these values are taken from [133] and are the same as adopted in Refs. [1, 89, 98].

The BDM flux from an individual SN arriving at Earth at time t' after the SN explosion occurs is computed by integrating over the solid angle (θ, φ) in the Earth-centered spherical coordinate system,

$$\frac{d\Phi_\chi(T_\chi, t')}{dT_\chi} = \tau_s \int_0^{2\pi} d\varphi \int_0^{\pi/2} d\theta \sin\theta \frac{d\Phi_\chi}{dT_\chi d\Omega}(r, d, T_\chi, \psi) \Big|_{t' = \frac{d}{c} + \frac{\ell}{v_\chi}}. \quad (11)$$

Note that the propagation time t' can be related to d and ℓ by

$$t' = \frac{d}{c} + \frac{\ell}{v_\chi} \quad (12)$$

with $d = \sqrt{R_s^2 + \ell^2 - 2R_s\ell \cos\theta}$. The integrand in Eq. (11)

$$\frac{d\Phi_\chi}{dT_\chi d\Omega} = \mathcal{J} j_\chi(r, d, T_\chi, \psi) \quad (13)$$

is the differential flux on the sky and

$$\mathcal{J} = \left(\frac{\ell - R_s \cos\theta}{cd} + \frac{1}{v_\chi} \right)^{-1} \quad (14)$$

is the Jacobian factor. We approximate τ_s by 10 s, which is the characteristic SN ν emission time scale. By defining a shifted time variable

$$t \equiv t' - t_\nu = \frac{d}{c} + \frac{\ell}{v_\chi} - t_\nu, \quad (15)$$

with $t_\nu = R_s/c$ being the SN ν travel time from S to E, we align $t = 0$ with the arrival time of SN ν at Earth.

As pointed out in Refs. [89, 98], the BDM flux from an individual SN lasts for a certain duration t_{van} before vanishing, which can be determined by

$$t_{\text{van}}(R_s, v_\chi) = \left[\frac{d(\theta)}{c} + \frac{\ell(\theta)}{v_\chi} - t_\nu \right]_{\theta=\theta^*}, \quad (16)$$

where θ^* satisfies

$$\frac{\cos(\psi_{\text{max}} - \theta^*)}{\cos\theta^*} = \frac{v_\chi}{c}. \quad (17)$$

In Eq. (17)

$$\psi_{\text{max}} = \cos^{-1} \left(\frac{T_\chi}{|\mathbf{p}_\chi|} \right) \leq \frac{\pi}{2} \quad (18)$$

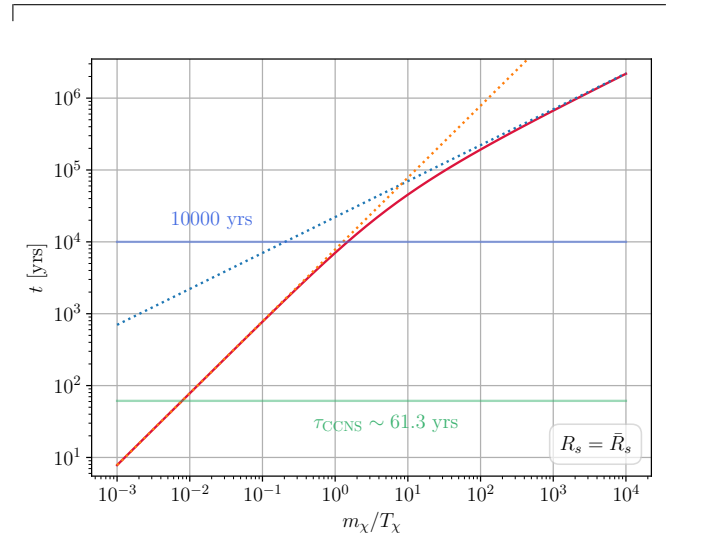


FIG. 4. t_{van} versus m_χ/T_χ evaluated at $R_s = \bar{R}_s \approx 9.6 \text{ kpc}$ (red). Also shown are the approximated solution of t_{van} from Eq. (19) in the nonrelativistic (blue dotted line) and relativistic (orange dotted line). Two horizontal solid lines corresponding to 10,000 yrs (blue) and τ_{CCNS} (green) are shown for reference.

is the maximum allowed scattering angle and $|\mathbf{p}_\chi| = \sqrt{T_\chi(T_\chi + 2m_\chi)}$. In the ultrarelativistic ($m_\chi/T_\chi \ll 1$) and nonrelativistic ($m_\chi/T_\chi \gg 1$) limits, t_{van} can be approximated by (see App. A for derivation)

$$t_{\text{van}}(R_s, v_\chi) \approx \begin{cases} \frac{m_\chi R_s}{4T_\chi c}, & m_\chi/T_\chi \ll 1, \\ \sqrt{\frac{m_\chi R_s}{2T_\chi c}}, & m_\chi/T_\chi \gg 1. \end{cases} \quad (19)$$

In addition to t_{van} , another important timescale defined in Ref. [89, 98] is

$$t_p(R_s, v_\chi) = \frac{R_s}{v_\chi} - t_\nu, \quad (20)$$

which corresponds to the delayed arrival time of BDM

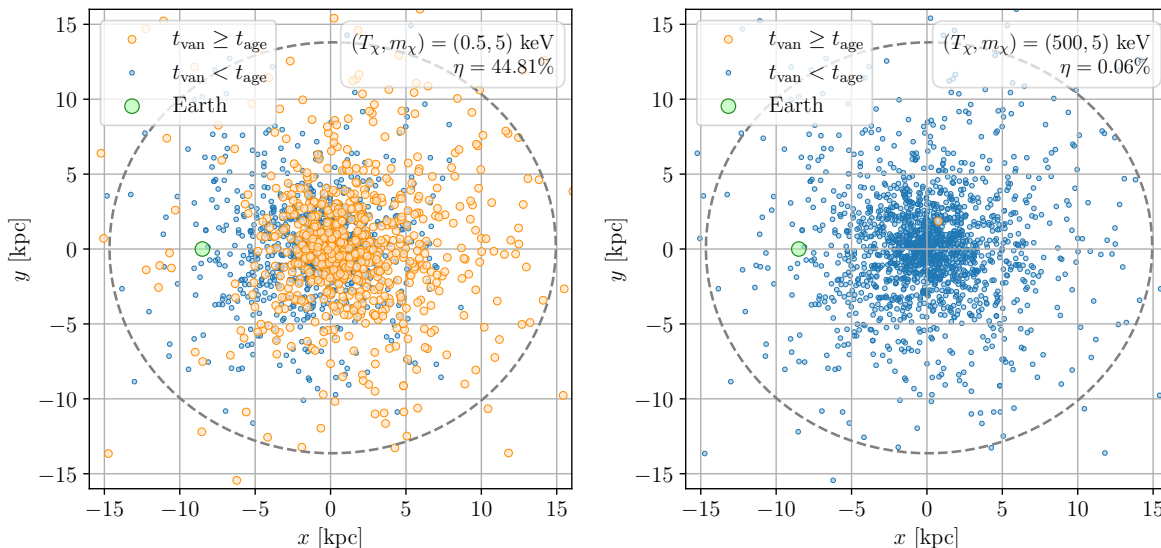


FIG. 5. Spatial distribution of SNe that contribute (orange circles) and do not contribute (blue circles) to the present-day BDM flux at Earth. $T_\chi = 0.5$ keV and 5 keV for the left and right panels. DM mass is taken to be $m_\chi = 5$ keV for both panels. η denotes the fraction of SNe contributing non-zero BDM flux from the whole data set.

from locations very close to the SN position after the arrival of the $\text{SN}\nu$.

To understand the characteristic t_{van} of $\text{SN}\nu$ BDM from MW for different v_χ (which can be related to m_χ/T_χ), we compute numerically $t_{\text{van}}(\bar{R}_s, v_\chi)$, shown by the red solid line in Fig. 4, for a SN that occurs at a distance away from the Earth given by the averaged distance weighted over the spatial distribution function p_{SN}

$$\bar{R}_s = \int dR dz d\phi R_s p_{\text{SN}}(R, z) \approx 9.6 \text{ kpc}, \quad (21)$$

where R_s is evaluated as

$$R_s = \sqrt{(R_\star \cos \phi_\star + R_e)^2 + R_\star^2 \sin^2 \phi_\star + z_\star^2} \quad (22)$$

with $(R_\star, z_\star, \phi_\star)$ being the SN location in the galactic coordinate (see Fig. 1). Also shown in Fig. 4 by the dotted lines are the approximate t_{van} evaluated with Eq. (19). Fig. 4 shows that for nonrelativistic case with $m_\chi/T_\chi = 10$, $t_{\text{van}}(\bar{R}_s) \simeq 4.5 \times 10^4$ yrs, implying that many SNe that happened during this time span with $t_{\text{van}} \geq t_{\text{age}}$ should still contribute to the present-day $\text{SN}\nu$ BDM flux. However, for the relativistic case with e.g., $m_\chi/T_\chi = 0.01$, $t_{\text{van}}(\bar{R}_s) \simeq 1.1\tau_{\text{CCSN}}$, i.e., the duration of the $\text{SN}\nu$ BDM is comparable to the averaged interval between successive SNe in MW. In this case, the $\text{SN}\nu$ BDM at Earth likely originates from very few SNe at any given time.

In Fig. 5, we indicate the SNe in our sample whose $t_{\text{van}} \geq t_{\text{age}}$ by filled orange dots shown in the projected x - y plane in the galactic coordinate (same as Fig. 2) for $(T_\chi, m_\chi) = (0.5, 5)$ and $(500, 5)$ keV, to support the above reasoning. The blue dots represent those SNe that do not contribute to the present-day BDM flux.

For $m_\chi/T_\chi = 10$ ($v_\chi \sim 0.4c$), the fraction of SNe with $t_{\text{van}} \geq t_{\text{age}}$, denoted by η , is 44.81% (left figure). This corresponds to a non-vanishing contribution of BDM from 747 SNe, confirming that a large fraction of past SNe in MW should contribute to the present-day BDM flux when considering nonrelativistic T_χ range. In contrast, for relativistic case with $m_\chi/T_\chi = 0.01$ (right figure), only 1 SN still produces nonzero BDM flux at Earth ($\eta \simeq 0.06\%$), confirming that when $t_{\text{van}}(\bar{R}_s) \simeq \tau_{\text{CCSN}}$, the $\text{SN}\nu$ BDM flux is dominated by at most few SNe.

Since t_{van} depends only on m_χ/T_χ , in what follows, we fix $m_\chi = 5$ keV and take different T_χ values between 0.5 keV and 5 MeV to explore the dependence of the temporal and angular profiles of $\text{SN}\nu$ BDM from our SN sample on m_χ/T_χ .

IV. NUMERICAL RESULTS

In the previous sections, we discussed how SNe are distributed in MW according to p_{SN} , and what fraction of them can contribute to a non-zero BDM flux at the present day. In this section, we first evaluate the temporal evolution of the BDM flux over the last $\sim \mathcal{O}(10^3)$ yrs by summing over all SN contributions, each of which being evaluated with Eq. (11) in Sec. IV A. In Sec. IV B, we further examine how present-day BDM flux is distributed across the celestial sphere using Eq. (13). In evaluating the fluxes from each SN, we have placed a minimal cutoff for d at $d_{\text{cut}} = 200$ km. While the choice of d_{cut} here is much smaller than the cutoffs chosen in Refs. [1, 89, 98], we have verified that a different choice only results in negligible changes to results presented here.

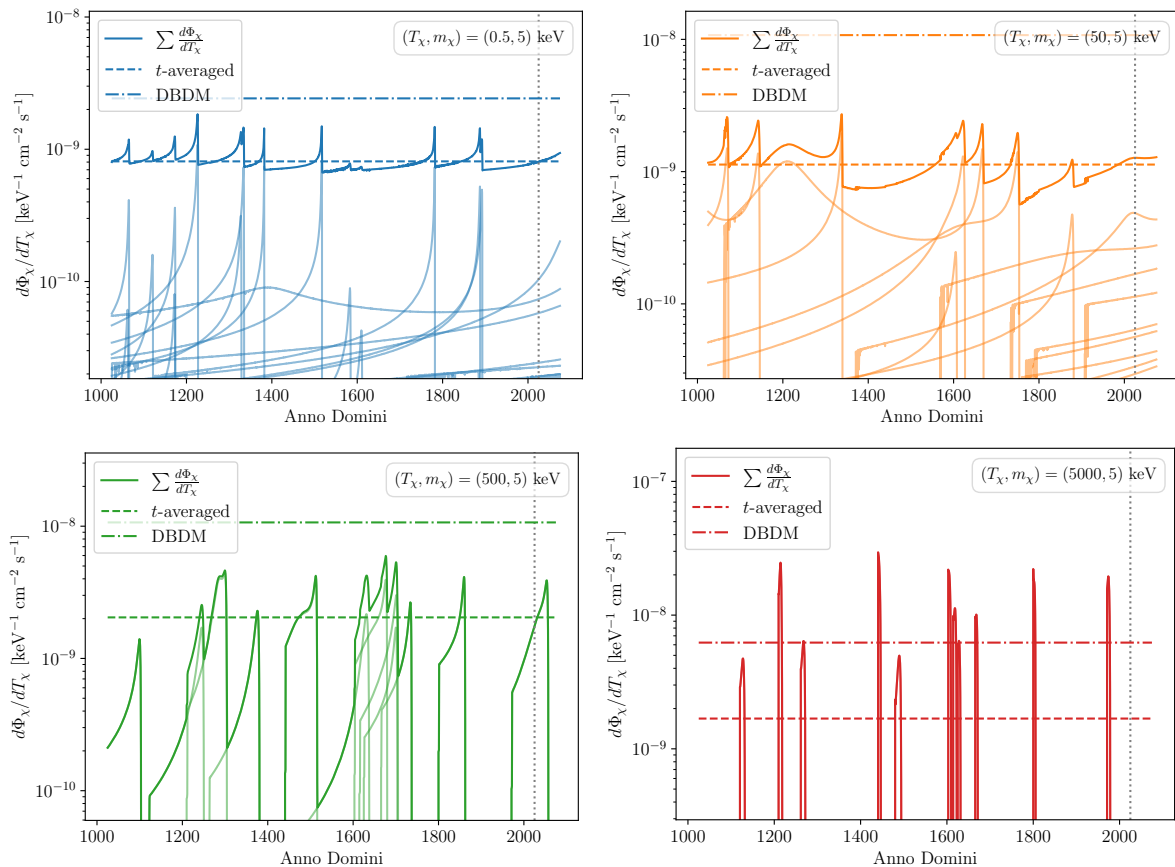


FIG. 6. Evolution of BDM fluxes from MW SNe in our mocked sample over a time span of one millennium. We take $m_\chi = 5$ keV, with different values of T_χ indicated in the top-right corner of each panel. The solid lines show the MW cumulative BDM flux (labeled by $\sum \frac{d\Phi_\chi}{dT_\chi}$) obtained by summing contributions from all individual MW SNe (light solid lines). The dashed lines represent the time-averaged BDM flux over the same duration shown in the plot. The dot-dashed lines show the DBDM flux from all SNe in galaxies at higher redshifts. Gray vertical dotted lines mark the present day, assuming year 2025.

A. Evolution of BDM flux

In Fig. 6, we show the BDM flux from each MW SN (curves with lighter colors) computed with Eq. (11) and the total flux summing over all MW SNe in our sample (darker colors; labeled by $\sum \frac{d\Phi_\chi}{dT_\chi}$), spanning from AD 1025 to AD 2075 for four representative values of $T_\chi = 0.5, 50, 500,$ and 5000 keV. The present day, assumed as year 2025, is marked by the gray dotted line. For each T_χ , we also plot the DBDM flux computed in Ref. [1] by dot-dashed line. From here onward, unless explicitly stated it is DBDM, the acronym BDM refers to those coming from the SNe in MW.

For $T_\chi = 0.5$ keV shown in the top left panel, corresponding to the same case shown in the left panel of Fig. 5, there are more than 700 SNe contributed to the present-day BDM flux since the average vanishing time of all 1,667 SNe in our dataset $\bar{t}_{\text{van}} \simeq 5.3 \times 10^4$ years².

However, even in this case, the total BDM flux still varies in time by a factor of ~ 3 . This is mainly because the BDM flux from each individual SN peaks close to t_{van} as clearly shown by curves with lighter colors. It is important to note that at low T_χ range with $T_\chi \ll \langle E_{\nu_i} \rangle$, the temporal behavior of the BDM flux is different from that for $T_\chi \gtrsim \langle E_{\nu_i} \rangle$, where the flux peaks at $\sim t_p$ when $\sigma_{\chi\nu}$ is energy-independent [89, 98]. We find that this is because when $T_\chi \ll \langle E_{\nu_i} \rangle$, BDM that arrives at later times are dominantly upscattered at locations closer to where the SN explodes. Meanwhile, the required neutrino energy for BDM stays nearly constant over time. Hence, $dn_\nu/dE_\nu \propto d^{-2}$ increases with time, leading to a larger BDM flux closer to t_{van} . On the other hand, when $T_\chi \gtrsim \langle E_{\nu_i} \rangle$, the required neutrino energy for BDM arriving at $t \gtrsim t_p$ increases with time and can largely exceed $\langle E_{\nu_i} \rangle$. In this case, the exponential suppression

² This value is similar to the characteristic value of $t_{\text{van}}(\bar{R}_s)$ eval-

uated for a representative SN at \bar{R}_s reported in the previous section for the same m_χ/T_χ .

of dn_ν/dE_ν at $E_\nu \gg \langle E_{\nu_i} \rangle$ results in decrease of the BDM flux for $t \gtrsim t_p$ reported in Refs. [89, 98]. More importantly, the BDM flux is not dominated by any single supernova, aside from the peaks. The BDM flux outside the short durations around the peaks differs from the time-averaged flux only by $\lesssim 15\%$ and may be approximated as a stationary component. In particular, the largest contribution from a single SN to the present-day BDM flux is only up to $\sim 13\%$.

As T_χ increases, the number of SNe contributing to the cumulative BDM flux decreases rapidly. The overlaps of BDM fluxes from individual SNe diminishes, resulting in a less steady total flux. For example, with $m_\chi/T_\chi = 0.1$ shown in the top right panel of Fig. 6, which corresponds to $t_{\text{van}} = 7.8 \times 10^2$ yrs, our SN sample yields BDM flux that varies in time by a factor of ~ 5 . At any given time, the total flux is dominated by only a few SNe such that the actual flux can differ from the time-averaged flux by a factor of ~ 2 . With an even smaller value of $m_\chi/T_\chi = 0.01$ (bottom left panel), which corresponds to $t_{\text{van}} \approx 79$ yrs $\approx 1.29\tau_{\text{CCSN}}$, the BDM flux generally differs from the time-averaged value by up to a factor of $\sim \mathcal{O}(10)$ for most of the times, and can even completely vanish at certain intervals. Finally, for the ultrarelativistic limit with $t_{\text{van}} \approx 7.9$ yrs $\approx 0.13\tau_{\text{CCSN}}$, t_{van} from individual SN only last for weeks to a few years after $\text{SN}\nu$ arrives. Thus, the BDM flux becomes nonzero only around the time when a SN explodes.

The above discussions suggest that only when $t_{\text{van}} \gg \tau_{\text{CCSN}}$, which corresponds to $m_\chi/T_\chi \gtrsim \mathcal{O}(10)$, the resulting BDM flux at Earth may be approximated as steady. In the next subsection, we will show that a similar criteria also applies to the angular distribution of BDM flux over the sky. Moreover, our results here show that the $\text{SN}\nu$ BDM flux only exceeds the DBDM flux in the ultrarelativistic case when $t_{\text{van}} \ll \tau_{\text{CCSN}}$, indicating that the diffuse component of $\text{SN}\nu$ BDM should be dominated by the contribution from all SNe at higher redshifts, but not from the past SNe in MW.

B. BDM angular distribution across the celestial sphere

After examining the temporal profile of angle-integrated $\text{SN}\nu$ BDM flux, we now investigate their angular distribution over the sky. We evaluate Eq. (13) and integrate over different T_χ ranges by

$$\frac{d\Phi_\chi(t)}{d\Omega} = \tau_s \int_{T_{\chi,\min}}^{T_{\chi,\max}} dT_\chi \left. \frac{d\Phi_\chi}{dT_\chi d\Omega} \right|_{t=\frac{d}{c} + \frac{e}{v_\chi} - t_\nu} \quad (23)$$

at any given time t . We fix $m_\chi = 5$ keV and consider two different ranges for T_χ for demonstration: $(T_{\chi,\min}, T_{\chi,\max}) = (1, 5)$, and $(300, 1000)$ keV. Left panels of Fig. 7 show the resulting distributions at present day ($t = 10^5$ years) considering the MW $\text{SN}\nu$ BDM only. For reference, we also mark the angular position

of three stars: Polaris, Sirius, and α Centauri, in each panel. Clearly, with low T_χ range in the nonrelativistic limit (upper left panel), the resulting BDM fluxes from individual SNe becomes very dispersive and extends to higher latitudes. This can be understood by examining the BDM angular distribution $g_\chi(\psi)$ versus the scattering angle ψ at a given boosted point (B) [Eq. (9)] for different values of m_χ/T_χ shown in Fig. 8. Clearly, the larger the m_χ/T_χ is, the more spread of the BDM flux across the sky. As a result, contributions from different SNe largely overlap, which gives rise to an overall larger flux toward the direction of GC. Although the figure also shows that the BDM flux peaks within a very small solid angle range centered at directions corresponding the location of contributing SNe, due to the larger value of dn_ν/dE_ν close to the SN location (see Eq. 10), it would require an extremely good angular resolution in experiments to isolate them. Thus, the BDM flux in this limit can be practically considered as spatially diffusive. On the other hand, for $300 \text{ keV} \leq T_\chi < 1000 \text{ keV}$ (bottom left panel), only 5 SNe close to the GC contribute to the BDM flux. If an angular resolution of a few degrees can be achieved, it is possible to separate contributions from individual SNe.

Note that the angular distribution of BDM from each SN exhibits a ring-like feature in both cases. This is related to the fact that BDM with larger scattering angle ψ is upscattered by neutrinos with higher E_ν ; see Eq. (A10) in Ref. [98]. For $T_\chi < 1 \text{ MeV} \ll \langle E_{\nu_i} \rangle$ considered in Fig. 7, dn_ν/dE_ν increases with E_ν^2 , resulting in larger BDM flux at larger ψ . The ring-like shape is clearly visible in the bottom left panel where the contributions of each SN are separated, but becomes obscured in the upper left panel at the diffuse limit.

In the right panels of Fig. 7, we show the expected angular distributions that include the DBDM component. Clearly, for the case with nonrelativistic T_χ range shown in the upper right panel, the contribution from the MW SNe only stands out from the isotropic DBDM flux within $\sim 10^\circ$ in latitude and $\sim 30^\circ$ in longitude around GC. Outside this angular range, the DBDM flux dominates. For the relativistic case (lower right panel), the BDM fluxes from individual SNe are generally larger than the DBDM flux. However, as the all-sky-integrated flux is dominated by DBDM (Fig. 6), it would also require good detection angular resolution at these T_χ ranges to uncover the BDM contribution due to the past MW SNe.

V. BDM FROM SUPERNOVA REMNANTS

So far we have focused on results obtained using the mocked SN dataset shown in Fig. 2. However, hundreds of SNRs have been observed and documented; see e.g., SNRcat [134] for a catalog. Here, we analyze the temporal and spatial BDM distributions resulting from this catalog with the provided SNR age, distance, and direction estimations as well as their associated remnant prop-

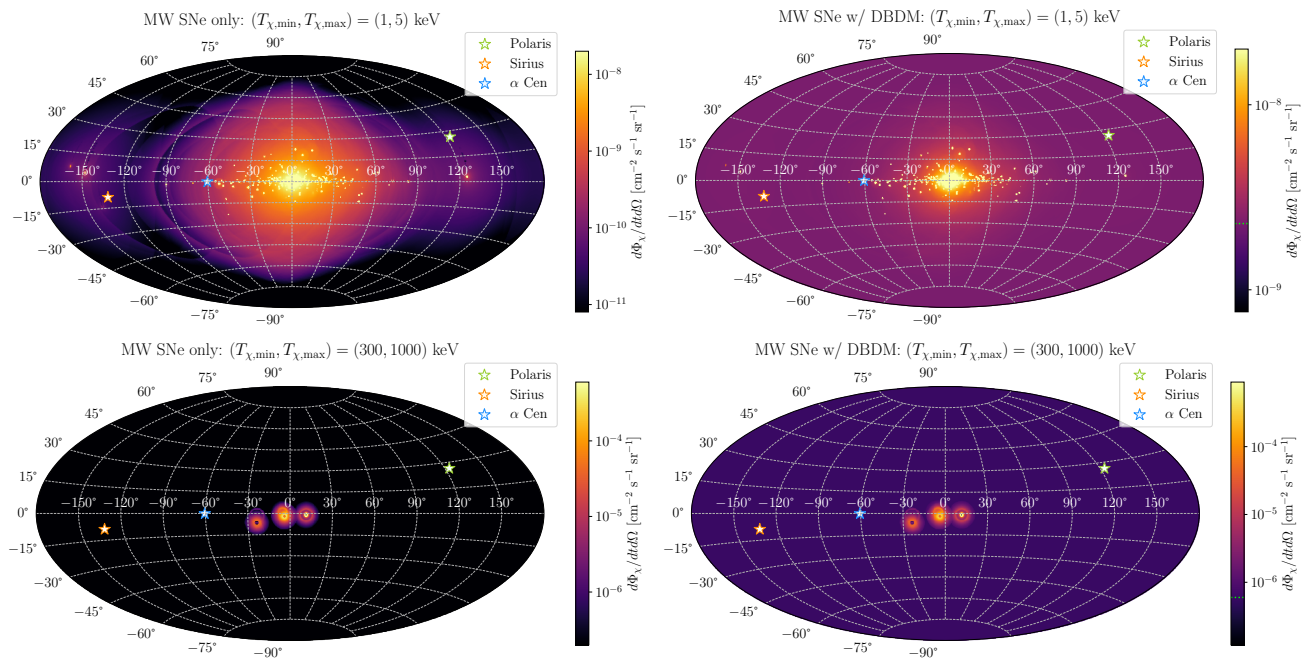


FIG. 7. T_χ -integrated BDM flux per steradian over the celestial sphere, in galactic coordinate, at present day for different T_χ ranges indicated by the labels. Left panels show the result that only considers MW SNe from our mocked dataset, while the right panels include contribution of DBDM, whose values are indicated by the short green dotted lines in the color bar (2.28×10^{-9} and $5.98 \times 10^{-7} \text{ cm}^{-2} \text{ s}^{-1} \text{ sr}^{-1}$ in the upper and lower panels, respectively). We assume $m_\chi = 5 \text{ keV}$ for both cases. The locations of three representative stars, Polaris, Sirius and α Centauri are marked by star symbols.

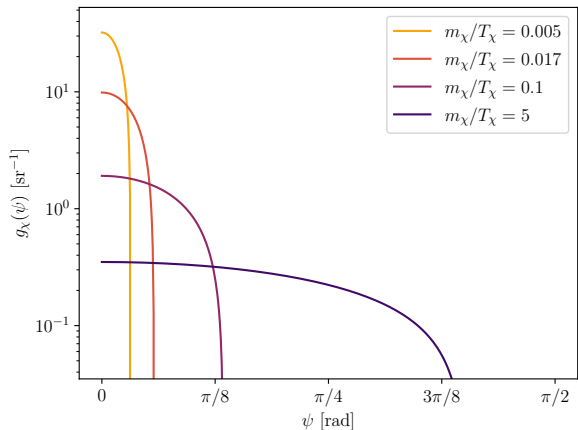


FIG. 8. The BDM angular distribution at boost point (B) for different m_χ/T_χ values.

erties. Because not all listed SNRs contain all above information needed to evaluation the corresponding BDM flux, we only consider SNRs with: (1) potential association with remnants classified as NS (neutron star), PSR (pulsar remnant), or PWN (pulsar wind nebula); and (2) identifiable age and distance. Given the large uncertainties in inferring the ages and distances of SNRs, we take the average of the reported minimum and maximum values as their true ages and distances. If only one single value is provided for age or distance, we use it as the

nominal one. After this selection, 81 SNRs remain in this “realistic” SN dataset. Among them, 77 SNRs have ages less than 100,000 yrs, with distances between 0.6 and 16.7 kpc. We then perform the same calculations to obtain the corresponding temporal and spatial BDM fluxes at the present day, which are shown in Figs. 9 and 10, respectively. Note that the number of SNe in this dataset is much smaller than that of the mock data mainly due to dust distinction as well as observational limits. Thus, the results presented below can be considered as the “floor” for BDM from MW’s past SNe.

For the temporal distribution shown in Fig. 9, we again take $T_\chi = 0.5$ (left panel) and 50 keV (right panel) and fix $m_\chi = 5 \text{ keV}$. Here, even with $m_\chi/T_\chi = 10$, the cumulative BDM flux does not exhibit the diffuse nature shown in the upper left panel of Fig. 6, due to limited number of identified SNRs. Except the two specific peaks between AD 1650 and AD 1850 associated with very nearby SNRs³, the flux is much smaller than the DBDM one. For $T_\chi = 50 \text{ keV}$ (right panel), the BDM flux sits completely under the DBDM flux all the time and is zero now.

For the BDM spatial distribution (Fig. 10), integrated

³ These two distinct peaks are from Vela Jr. (G266.2–01.2) and Boomerang (G106.3+02.7), both of which are located approximately 0.75 kpc from Earth and are estimated to be 3750 and 3900 year-old, respectively.

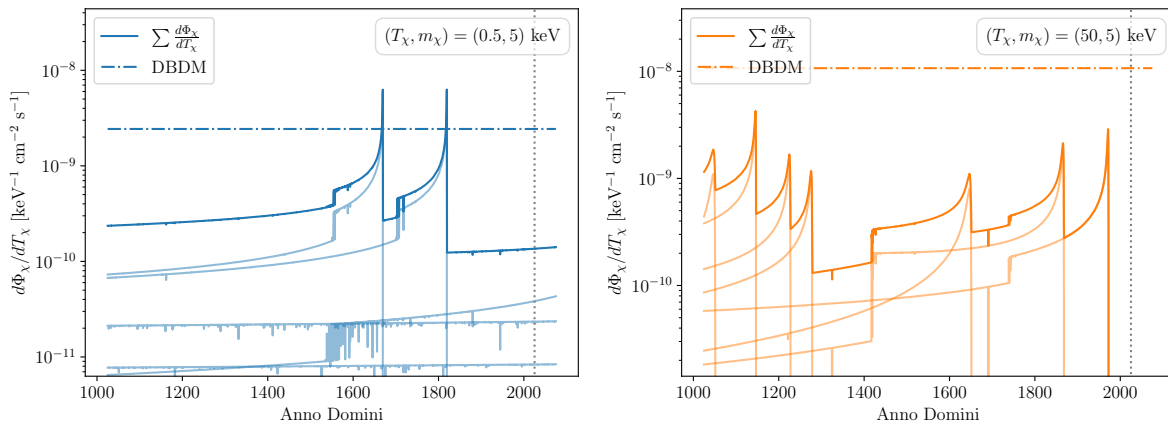


FIG. 9. Time evolution of BDM fluxes from SNe possibly associated with known SNRs over a time span of one millennium (see text for details). The same line styles of Fig. 6 are used to denote quantities shown in the plots.

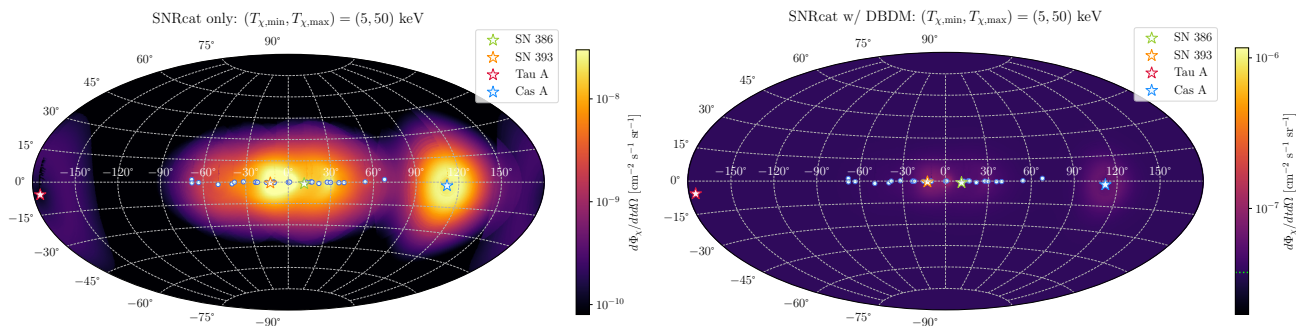


FIG. 10. T_χ -integrated BDM flux per steradian over the celestial sphere, in galactic coordinate, at present day, from SNe possibly associated with known SNRs for $m_\chi = 5$ keV. The Left and the right panel shows the result that only considers MW SNe and the values including DBDM contribution (indicated by the green dotted line with a value of $3.76 \times 10^{-8} \text{ cm}^{-2} \text{ s}^{-1} \text{ sr}^{-1}$ on the color bar of the right panel), respectively. Locations of SNe that contribute to the BDM flux are labeled by the blue dots. Four known SNe in recent history are marked by star symbols.

over a T_χ range within $(T_{\chi,\text{min}}, T_{\chi,\text{max}}) = (5, 50)$ keV, the DBDM contribution is excluded (included) in the left (right) panel. The locations of SNe whose contributions are nonzero are marked by blue dots. Four specific remnants: SN 386 (G011.2–00.3), SN 393 (G347.3–00.5), Taurus A (G184.6–05.8, aka the Crab Nebula), and Cassiopeia A (G111.7–02.1) are particularly labeled by star symbols for reference. With this T_χ range, the BDM flux from each SN spreads widely over the sky and overlaps with each other. However, once the DBDM flux is considered, the BDM flux are mostly buried under the DBDM, except for those around Taurus A and Cassiopeia A. We do not show results in larger T_χ range. This is because in that case, the ages of all SNe in this dataset are greater than their t_{van} such that they cannot contribute to the present-day flux.

VI. SUMMARY

In this work, we have investigated the temporal and spatial distribution of the $\text{SN}\nu$ BDM flux for BDM with low kinetic energy T_χ such that the typical BDM flux duration, t_{van} , from a single galactic SN is comparable to or larger than the typical time interval between two successive SNe. Due to insufficient information of all SNe in the MW history, we rely on MC simulation to generate a mock dataset that contains the locations and ages of 1,667 SNe over a time span of 100,000 yrs. Using this dataset, we computed the detailed time evolution of the angle-integrated BDM flux for different values of m_χ/T_χ covering both the nonrelativistic and the relativistic limits. We find that for nonrelativistic BDM whose $m_\chi/T_\chi = 10$, BDM from over 44% of SNe in our dataset still contribute to the present-day flux. We have also shown that in this case, the accumulated $\text{SN}\nu$ BDM varies within $\sim 15\%$ of their time-averaged value, except for short durations where the flux from individual SN peaks. Thus, for most of the time, the time-averaged

SN ν BDM flux can be taken as a good approximation. However, for relativistic SN ν BDM with $m_\chi/T_\chi < 0.1$, corresponding to a typical $t_{\text{van}} > \mathcal{O}(800)$ yrs, the variation of their temporal flux is generally large and cannot be well approximated by steady-state approximation. This implies that when considering the SN ν BDM with sub-MeV T_χ relevant to e.g., semi-conductor-based DM searchers as done in Ref. [102], this effect can become important and cannot be neglected in determining the BDM flux originated from the past SNe in MW.

We have also evaluated the angular distribution of the same SN ν BDM flux at present. We find that it can be considered as diffuse for the nonrelativistic BDM, since the contribution of individual SNe are dispersed over a large sky area and overlap with each other. On the other hand, the BDM flux from different SNe may be discerned given enough angular resolution in the relativistic regime. For completeness, we have also utilized available SNR data, which have about 80 SNRs potentially associated with CCSNe to estimate the corresponding BDM flux.

Comparing the BDM flux from past SNe in MW to the DBDM flux originated from all SNe in galaxies at higher redshifts investigated in Ref. [1], we find that for $m_\chi/T_\chi \gtrsim 0.01$, the all-sky-integrated MW SN ν BDM flux is generally smaller than the DBDM flux by a factor

of a few. Although the MW BDM flux in certain angular domains can be larger than the isotropic DBDM flux, it would require relevant experiments to achieve angular resolution of $\mathcal{O}(10)$ degree to uncover the MW SN ν BDM flux with sub-MeV kinetic energy. This finding suggests that DBDM should be considered as the primary target for relevant searches of SN ν BDM before the next galactic SN takes place. When such an once-in-a-lifetime event happens, the transient feature of SN ν BDM at $T_\chi \gtrsim \mathcal{O}(1)$ MeV originally proposed in Ref. [89] will possibly allow various neutrino and DM experiments to better probe the nature of DM in complementary to many other ways.

ACKNOWLEDGMENTS

We thank Bin Zhu for useful discussions. YHL and MRW acknowledge support from the National Science and Technology Council, Taiwan under Grant No. 111-2628-M-001-003-MY4, the Academia Sinica under Project No. AS-IV-114-M04, and Physics Division, National Center for Theoretical Sciences of Taiwan. We would like to also acknowledge the use of computational resources provided by the Academia Sinica Grid-computing Center.

-
- [1] Y.-H. Lin and M.-R. Wu, *Phys. Rev. Lett.* **133**, 111004 (2024), [arXiv:2404.08528 \[hep-ph\]](#).
 - [2] K. Choi, S. H. Im, and C. Sub Shin, *Ann. Rev. Nucl. Part. Sci.* **71**, 225 (2021), [arXiv:2012.05029 \[hep-ph\]](#).
 - [3] G. Arcadi, M. Dutra, P. Ghosh, M. Lindner, Y. Mambrini, M. Pierre, S. Profumo, and F. S. Queiroz, *Eur. Phys. J. C* **78**, 203 (2018), [arXiv:1703.07364 \[hep-ph\]](#).
 - [4] D. S. Akerib *et al.* (LUX), *Phys. Rev. Lett.* **118**, 021303 (2017), [arXiv:1608.07648 \[astro-ph.CO\]](#).
 - [5] D. S. Akerib *et al.* (LUX), *Phys. Rev. Lett.* **118**, 251302 (2017), [arXiv:1705.03380 \[astro-ph.CO\]](#).
 - [6] R. Agnese *et al.* (SuperCDMS), *Phys. Rev. Lett.* **121**, 051301 (2018), [Erratum: *Phys.Rev.Lett.* **122**, 069901 (2019)], [arXiv:1804.10697 \[hep-ex\]](#).
 - [7] E. Aprile *et al.* (XENON), *Phys. Rev. Lett.* **121**, 111302 (2018), [arXiv:1805.12562 \[astro-ph.CO\]](#).
 - [8] E. Aprile *et al.* (XENON), *Phys. Rev. Lett.* **123**, 251801 (2019), [arXiv:1907.11485 \[hep-ex\]](#).
 - [9] E. Aprile *et al.* (XENON), *Phys. Rev. Lett.* **123**, 241803 (2019), [arXiv:1907.12771 \[hep-ex\]](#).
 - [10] O. Abramoff *et al.* (SENSEI), *Phys. Rev. Lett.* **122**, 161801 (2019), [arXiv:1901.10478 \[hep-ex\]](#).
 - [11] M. Aguilar *et al.* (AMS), *Phys. Rev. Lett.* **115**, 211101 (2015).
 - [12] M. G. Aartsen *et al.* (IceCube), *Eur. Phys. J. C* **77**, 146 (2017), [Erratum: *Eur.Phys.J.C* **79**, 214 (2019)], [arXiv:1612.05949 \[astro-ph.HE\]](#).
 - [13] M. Ackermann *et al.* (Fermi-LAT), *Astrophys. J.* **840**, 43 (2017), [arXiv:1704.03910 \[astro-ph.HE\]](#).
 - [14] R. Abbasi *et al.* (IceCube), *Phys. Rev. D* **105**, 062004 (2022), [arXiv:2111.09970 \[astro-ph.HE\]](#).
 - [15] R. Abbasi *et al.* (IceCube), *Phys. Rev. D* **108**, 102004 (2023), [arXiv:2303.13663 \[astro-ph.HE\]](#).
 - [16] I. John, R. K. Leane, and T. Linden, (2023), [arXiv:2311.16228 \[astro-ph.HE\]](#).
 - [17] R. Abbasi *et al.* (IceCube), (2024), [arXiv:2412.12972 \[astro-ph.HE\]](#).
 - [18] L. Marsicano, M. Battaglieri, M. Bondi, C. D. R. Carvajal, A. Celentano, M. De Napoli, R. De Vita, E. Nardi, M. Raggi, and P. Valente, *Phys. Rev. Lett.* **121**, 041802 (2018), [arXiv:1807.05884 \[hep-ex\]](#).
 - [19] A. Boveia and C. Doglioni, *Ann. Rev. Nucl. Part. Sci.* **68**, 429 (2018), [arXiv:1810.12238 \[hep-ex\]](#).
 - [20] Y. Hochberg, Y. F. Kahn, R. K. Leane, S. Rajendran, K. Van Tilburg, T.-T. Yu, and K. M. Zurek, *Nature Rev. Phys.* **4**, 637 (2022).
 - [21] R. Essig, J. Mardon, and T. Volansky, *Phys. Rev. D* **85**, 076007 (2012), [arXiv:1108.5383 \[hep-ph\]](#).
 - [22] P. W. Graham, D. E. Kaplan, S. Rajendran, and M. T. Walters, *Phys. Dark Univ.* **1**, 32 (2012), [arXiv:1203.2531 \[hep-ph\]](#).
 - [23] R. Essig, M. Fernandez-Serra, J. Mardon, A. Soto, T. Volansky, and T.-T. Yu, *JHEP* **05**, 046 (2016), [arXiv:1509.01598 \[hep-ph\]](#).
 - [24] Y. Hochberg, Y. Zhao, and K. M. Zurek, *Phys. Rev. Lett.* **116**, 011301 (2016), [arXiv:1504.07237 \[hep-ph\]](#).
 - [25] Y. Hochberg, M. Pyle, Y. Zhao, and K. M. Zurek, *JHEP* **08**, 057 (2016), [arXiv:1512.04533 \[hep-ph\]](#).
 - [26] Y. Hochberg, I. Charaev, S.-W. Nam, V. Verma, M. Colangelo, and K. K. Berggren, *Phys. Rev. Lett.* **123**, 151802 (2019), [arXiv:1903.05101 \[hep-ph\]](#).
 - [27] Y. Hochberg, E. D. Kramer, N. Kurinsky, and B. V.

- Lehmann, (2021), [arXiv:2109.04473 \[hep-ph\]](#).
- [28] Y. Hochberg, B. V. Lehmann, I. Charaev, J. Chiles, M. Colangelo, S. W. Nam, and K. K. Berggren, *Phys. Rev. D* **106**, 112005 (2022), [arXiv:2110.01586 \[hep-ph\]](#).
- [29] S. Derenzo, R. Essig, A. Massari, A. Soto, and T.-T. Yu, *Phys. Rev. D* **96**, 016026 (2017), [arXiv:1607.01009 \[hep-ph\]](#).
- [30] K. Schutz and K. M. Zurek, *Phys. Rev. Lett.* **117**, 121302 (2016), [arXiv:1604.08206 \[hep-ph\]](#).
- [31] Y. Hochberg, Y. Kahn, M. Lisanti, C. G. Tully, and K. M. Zurek, *Phys. Lett. B* **772**, 239 (2017), [arXiv:1606.08849 \[hep-ph\]](#).
- [32] R. Essig, J. Mardon, O. Slone, and T. Volansky, *Phys. Rev. D* **95**, 056011 (2017), [arXiv:1608.02940 \[hep-ph\]](#).
- [33] Y. Hochberg, Y. Kahn, M. Lisanti, K. M. Zurek, A. G. Grushin, R. Ilan, S. M. Griffin, Z.-F. Liu, S. F. Weber, and J. B. Neaton, *Phys. Rev. D* **97**, 015004 (2018), [arXiv:1708.08929 \[hep-ph\]](#).
- [34] G. Cavoto, F. Luchetta, and A. D. Polosa, *Phys. Lett. B* **776**, 338 (2018), [arXiv:1706.02487 \[hep-ph\]](#).
- [35] S. Griffin, S. Knapen, T. Lin, and K. M. Zurek, *Phys. Rev. D* **98**, 115034 (2018), [arXiv:1807.10291 \[hep-ph\]](#).
- [36] M.-A. Sánchez-Martínez, I. n. Robredo, A. Bidauzarraga, A. Bergara, F. de Juan, A. G. Grushin, and M. G. Vergniory, *Materials* **3**, 014001 (2019), [arXiv:1905.04805 \[cond-mat.mtrl-sci\]](#).
- [37] R. Essig, J. Pradler, M. Sholapurkar, and T.-T. Yu, *Phys. Rev. Lett.* **124**, 021801 (2020), [arXiv:1908.10881 \[hep-ph\]](#).
- [38] T. Emken, R. Essig, C. Kouvaris, and M. Sholapurkar, *JCAP* **09**, 070 (2019), [arXiv:1905.06348 \[hep-ph\]](#).
- [39] N. A. Kurinsky, T. C. Yu, Y. Hochberg, and B. Cabrera, *Phys. Rev. D* **99**, 123005 (2019), [arXiv:1901.07569 \[hep-ex\]](#).
- [40] C. Blanco, J. I. Collar, Y. Kahn, and B. Lillard, *Phys. Rev. D* **101**, 056001 (2020), [arXiv:1912.02822 \[hep-ph\]](#).
- [41] S. M. Griffin, Y. Hochberg, K. Inzani, N. Kurinsky, T. Lin, and T. Chin, *Phys. Rev. D* **103**, 075002 (2021), [arXiv:2008.08560 \[hep-ph\]](#).
- [42] C. Blanco, Y. Kahn, B. Lillard, and S. D. McDermott, *Phys. Rev. D* **104**, 036011 (2021), [arXiv:2103.08601 \[hep-ph\]](#).
- [43] D. Baxter, Y. Kahn, and G. Krnjaic, *Phys. Rev. D* **101**, 076014 (2020), [arXiv:1908.00012 \[hep-ph\]](#).
- [44] N. Kurinsky, D. Baxter, Y. Kahn, and G. Krnjaic, *Phys. Rev. D* **102**, 015017 (2020), [arXiv:2002.06937 \[hep-ph\]](#).
- [45] R. M. Geilhufe, F. Kahlhoefer, and M. W. Winkler, *Phys. Rev. D* **101**, 055005 (2020), [arXiv:1910.02091 \[hep-ph\]](#).
- [46] T. Emken, C. Kouvaris, and I. M. Shoemaker, *Phys. Rev. D* **96**, 015018 (2017), [arXiv:1702.07750 \[hep-ph\]](#).
- [47] T. Emken and C. Kouvaris, *JCAP* **10**, 031 (2017), [arXiv:1706.02249 \[hep-ph\]](#).
- [48] R. Catena, T. Emken, N. A. Spaldin, and W. Tarantino, *Phys. Rev. Res.* **2**, 033195 (2020), [Erratum: *Phys.Rev.Res.* **7**, 019001 (2025)], [arXiv:1912.08204 \[hep-ph\]](#).
- [49] A. Radick, A.-M. Taki, and T.-T. Yu, *JCAP* **02**, 004 (2021), [arXiv:2011.02493 \[hep-ph\]](#).
- [50] G. B. Gelmini, V. Takhistov, and E. Vitagliano, *Phys. Lett. B* **809**, 135779 (2020), [arXiv:2006.13909 \[hep-ph\]](#).
- [51] T. Trickle, Z. Zhang, and K. M. Zurek, *Phys. Rev. D* **105**, 015001 (2022), [arXiv:2009.13534 \[hep-ph\]](#).
- [52] S. Knapen, J. Kozaczk, and T. Lin, *Phys. Rev. D* **104**, 015031 (2021), [arXiv:2101.08275 \[hep-ph\]](#).
- [53] C. Cook, C. Blanco, and J. Smirnov, (2024), [arXiv:2501.00091 \[hep-ph\]](#).
- [54] A. Simchony *et al.*, *J. Low Temp. Phys.* **216**, 363 (2024).
- [55] R. Essig, G. K. Giovanetti, N. Kurinsky, D. McKinsey, K. Ramanathan, K. Stifter, and T.-T. Yu, in *2022 Snowmass Summer Study* (2022) [arXiv:2203.08297 \[hep-ph\]](#).
- [56] A. Das, N. Kurinsky, and R. K. Leane, *Phys. Rev. Lett.* **132**, 121801 (2024), [arXiv:2210.09313 \[hep-ph\]](#).
- [57] A. Das, N. Kurinsky, and R. K. Leane, *JHEP* **07**, 233 (2024), [arXiv:2405.00112 \[hep-ph\]](#).
- [58] S. M. Griffin, G. D. Hadas, Y. Hochberg, K. Inzani, and B. V. Lehmann, (2024), [arXiv:2412.16283 \[hep-ph\]](#).
- [59] L. Baudis *et al.* (QROCODILE), (2024), [arXiv:2412.16279 \[hep-ph\]](#).
- [60] G. Marocco and J. Wheeler, (2025), [arXiv:2501.18120 \[hep-ph\]](#).
- [61] R. K. Leane and J. F. Beacom, (2025), [arXiv:2503.09685 \[hep-ph\]](#).
- [62] H. An, M. Pospelov, J. Pradler, and A. Ritz, *Phys. Rev. Lett.* **120**, 141801 (2018), [Erratum: *Phys.Rev.Lett.* **121**, 259903 (2018)], [arXiv:1708.03642 \[hep-ph\]](#).
- [63] T. Bringmann and M. Pospelov, *Phys. Rev. Lett.* **122**, 171801 (2019), [arXiv:1810.10543 \[hep-ph\]](#).
- [64] Y. Ema, F. Sala, and R. Sato, *Phys. Rev. Lett.* **122**, 181802 (2019), [arXiv:1811.00520 \[hep-ph\]](#).
- [65] C. V. Cappiello and J. F. Beacom, *Phys. Rev. D* **100**, 103011 (2019), [Erratum: *Phys.Rev.D* **104**, 069901 (2021)], [arXiv:1906.11283 \[hep-ph\]](#).
- [66] J. B. Dent, B. Dutta, J. L. Newstead, and I. M. Shoemaker, *Phys. Rev. D* **101**, 116007 (2020), [arXiv:1907.03782 \[hep-ph\]](#).
- [67] W. Wang, L. Wu, J. M. Yang, H. Zhou, and B. Zhu, *JHEP* **12**, 072 (2020), [Erratum: *JHEP* **02**, 052 (2021)], [arXiv:1912.09904 \[hep-ph\]](#).
- [68] Y. Zhang, *PTEP* **2022**, 013B05 (2022), [arXiv:2001.00948 \[hep-ph\]](#).
- [69] G. Guo, Y.-L. S. Tsai, and M.-R. Wu, *JCAP* **10**, 049 (2020), [arXiv:2004.03161 \[astro-ph.HE\]](#).
- [70] S.-F. Ge, J. Liu, Q. Yuan, and N. Zhou, *Phys. Rev. Lett.* **126**, 091804 (2021), [arXiv:2005.09480 \[hep-ph\]](#).
- [71] Q.-H. Cao, R. Ding, and Q.-F. Xiang, *Chin. Phys. C* **45**, 045002 (2021), [arXiv:2006.12767 \[hep-ph\]](#).
- [72] Y. Jho, J.-C. Park, S. C. Park, and P.-Y. Tseng, *Phys. Lett. B* **811**, 135863 (2020), [arXiv:2006.13910 \[hep-ph\]](#).
- [73] W. Cho, K.-Y. Choi, and S. M. Yoo, *Phys. Rev. D* **102**, 095010 (2020), [arXiv:2007.04555 \[hep-ph\]](#).
- [74] Z.-H. Lei, J. Tang, and B.-L. Zhang, (2020), [arXiv:2008.07116 \[hep-ph\]](#).
- [75] G. Guo, Y.-L. S. Tsai, M.-R. Wu, and Q. Yuan, *Phys. Rev. D* **102**, 103004 (2020), [arXiv:2008.12137 \[astro-ph.HE\]](#).
- [76] C. Xia, Y.-H. Xu, and Y.-F. Zhou, *Nucl. Phys. B* **969**, 115470 (2021), [arXiv:2009.00353 \[hep-ph\]](#).
- [77] J. B. Dent, B. Dutta, J. L. Newstead, I. M. Shoemaker, and N. T. Arellano, *Phys. Rev. D* **103**, 095015 (2021), [arXiv:2010.09749 \[hep-ph\]](#).
- [78] Y. Ema, F. Sala, and R. Sato, *SciPost Phys.* **10**, 072 (2021), [arXiv:2011.01939 \[hep-ph\]](#).
- [79] V. V. Flambaum, L. Su, L. Wu, and B. Zhu, (2020), [arXiv:2012.09751 \[hep-ph\]](#).
- [80] Y. Jho, J.-C. Park, S. C. Park, and P.-Y. Tseng, (2021), [arXiv:2101.11262 \[hep-ph\]](#).

- [81] A. Das and M. Sen, *Phys. Rev. D* **104**, 075029 (2021), [arXiv:2104.00027](https://arxiv.org/abs/2104.00027) [hep-ph].
- [82] N. F. Bell, J. B. Dent, B. Dutta, S. Ghosh, J. Kumar, J. L. Newstead, and I. M. Shoemaker, *Phys. Rev. D* **104**, 076020 (2021), [arXiv:2108.00583](https://arxiv.org/abs/2108.00583) [hep-ph].
- [83] W. Chao, T. Li, and J. Liao, (2021), [arXiv:2108.05608](https://arxiv.org/abs/2108.05608) [hep-ph].
- [84] D. Ghosh, A. Guha, and D. Sachdeva, *Phys. Rev. D* **105**, 103029 (2022), [arXiv:2110.00025](https://arxiv.org/abs/2110.00025) [hep-ph].
- [85] J.-C. Feng, X.-W. Kang, C.-T. Lu, Y.-L. S. Tsai, and F.-S. Zhang, *JHEP* **04**, 080 (2022), [arXiv:2110.08863](https://arxiv.org/abs/2110.08863) [hep-ph].
- [86] W. Wang, L. Wu, W.-N. Yang, and B. Zhu, (2021), [arXiv:2111.04000](https://arxiv.org/abs/2111.04000) [hep-ph].
- [87] C. Xia, Y.-H. Xu, and Y.-F. Zhou, *JCAP* **02**, 028 (2022), [arXiv:2111.05559](https://arxiv.org/abs/2111.05559) [hep-ph].
- [88] J.-W. Wang, A. Granelli, and P. Ullio, *Phys. Rev. Lett.* **128**, 221104 (2022), [arXiv:2111.13644](https://arxiv.org/abs/2111.13644) [astro-ph.HE].
- [89] Y.-H. Lin, W.-H. Wu, M.-R. Wu, and H. T.-K. Wong, *Phys. Rev. Lett.* **130**, 111002 (2023), [arXiv:2206.06864](https://arxiv.org/abs/2206.06864) [hep-ph].
- [90] K. Abe *et al.* (Super-Kamiokande), *Phys. Rev. Lett.* **130**, 031802 (2023), [arXiv:2209.14968](https://arxiv.org/abs/2209.14968) [hep-ex].
- [91] X. Cui *et al.* (PandaX-II), *Phys. Rev. Lett.* **128**, 171801 (2022), [arXiv:2112.08957](https://arxiv.org/abs/2112.08957) [hep-ex].
- [92] R. Xu *et al.* (CDEX), (2022), [arXiv:2201.01704](https://arxiv.org/abs/2201.01704) [hep-ex].
- [93] A. Granelli, P. Ullio, and J.-W. Wang, (2022), [arXiv:2202.07598](https://arxiv.org/abs/2202.07598) [astro-ph.HE].
- [94] J. M. Cline, S. Gao, F. Guo, Z. Lin, S. Liu, M. Puel, P. Todd, and T. Xiao, *Phys. Rev. Lett.* **130**, 091402 (2023), [arXiv:2209.02713](https://arxiv.org/abs/2209.02713) [hep-ph].
- [95] C. Xia, Y.-H. Xu, and Y.-F. Zhou, *Phys. Rev. D* **107**, 055012 (2023), [arXiv:2206.11454](https://arxiv.org/abs/2206.11454) [hep-ph].
- [96] C. V. Cappiello, N. P. A. Kozar, and A. C. Vincent, *Phys. Rev. D* **107**, 035003 (2023), [arXiv:2210.09448](https://arxiv.org/abs/2210.09448) [hep-ph].
- [97] P. Carezza and P. De la Torre Luque, *Eur. Phys. J. C* **83**, 110 (2023), [arXiv:2210.17206](https://arxiv.org/abs/2210.17206) [astro-ph.HE].
- [98] Y.-H. Lin, T.-H. Tsai, G.-L. Lin, H. T.-K. Wong, and M.-R. Wu, *Phys. Rev. D* **108**, 083013 (2023), [arXiv:2307.03522](https://arxiv.org/abs/2307.03522) [hep-ph].
- [99] W. Wang, W.-L. Xu, J. M. Yang, and R. Zhu, (2023), [arXiv:2305.12668](https://arxiv.org/abs/2305.12668) [hep-ph].
- [100] G. Adhikari *et al.* (COSINE-100), (2023), [arXiv:2306.00322](https://arxiv.org/abs/2306.00322) [hep-ex].
- [101] C. Xia, C.-Y. Xing, and Y.-H. Xu, (2024), [arXiv:2401.03772](https://arxiv.org/abs/2401.03772) [hep-ph].
- [102] J.-W. Sun, L. Wu, Y.-H. Xu, and B. Zhu, (2025), [arXiv:2501.07591](https://arxiv.org/abs/2501.07591) [hep-ph].
- [103] K. Abe *et al.* (Super-Kamiokande), *Phys. Rev. D* **94**, 052010 (2016), [arXiv:1606.07538](https://arxiv.org/abs/1606.07538) [hep-ex].
- [104] K. Abe *et al.* (Hyper-Kamiokande), (2018), [arXiv:1805.04163](https://arxiv.org/abs/1805.04163) [physics.ins-det].
- [105] B. Abi *et al.* (DUNE), (2020), [arXiv:2002.03005](https://arxiv.org/abs/2002.03005) [hep-ex].
- [106] A. Abusleme *et al.* (JUNO), *Prog. Part. Nucl. Phys.* **123**, 103927 (2022), [arXiv:2104.02565](https://arxiv.org/abs/2104.02565) [hep-ex].
- [107] S. Horiuchi, J. F. Beacom, and E. Dwek, *Phys. Rev. D* **79**, 083013 (2009), [arXiv:0812.3157](https://arxiv.org/abs/0812.3157) [astro-ph].
- [108] J. F. Beacom, *Ann. Rev. Nucl. Part. Sci.* **60**, 439 (2010), [arXiv:1004.3311](https://arxiv.org/abs/1004.3311) [astro-ph.HE].
- [109] G. Chauhan, R. A. Gustafson, G. Herrera, T. Johnson, and I. Shoemaker, (2025), [arXiv:2505.03882](https://arxiv.org/abs/2505.03882) [hep-ph].
- [110] <https://github.com/yehsunlin/snorer/>.
- [111] <https://yehsunlin.github.io/snorer/>.
- [112] K. Rozwadowska, F. Vissani, and E. Cappellaro, *New Astron.* **83**, 101498 (2021), [arXiv:2009.03438](https://arxiv.org/abs/2009.03438) [astro-ph.HE].
- [113] P. J. McMillan, *Mon. Not. Roy. Astron. Soc.* **465**, 76 (2016), [arXiv:1608.00971](https://arxiv.org/abs/1608.00971) [astro-ph.GA].
- [114] <https://github.com/dfm/emcee/>.
- [115] X.-G. He, G. C. Joshi, H. Lew, and R. R. Volkas, *Phys. Rev. D* **44**, 2118 (1991).
- [116] P. J. Fox and E. Poppitz, *Phys. Rev. D* **79**, 083528 (2009), [arXiv:0811.0399](https://arxiv.org/abs/0811.0399) [hep-ph].
- [117] A. Falkowski, J. Juknevich, and J. Shelton, (2009), [arXiv:0908.1790](https://arxiv.org/abs/0908.1790) [hep-ph].
- [118] M. Lindner, A. Merle, and V. Niro, *Phys. Rev. D* **82**, 123529 (2010), [arXiv:1005.3116](https://arxiv.org/abs/1005.3116) [hep-ph].
- [119] H. Davoudiasl, H.-S. Lee, and W. J. Marciano, *Phys. Rev. D* **85**, 115019 (2012), [arXiv:1203.2947](https://arxiv.org/abs/1203.2947) [hep-ph].
- [120] S. Chang, R. Edezhath, J. Hutchinson, and M. Luty, *Phys. Rev. D* **90**, 015011 (2014), [arXiv:1402.7358](https://arxiv.org/abs/1402.7358) [hep-ph].
- [121] V. Gonzalez Macias and J. Wudka, *JHEP* **07**, 161 (2015), [arXiv:1506.03825](https://arxiv.org/abs/1506.03825) [hep-ph].
- [122] M. Battaglieri *et al.*, (2017), [arXiv:1707.04591](https://arxiv.org/abs/1707.04591) [hep-ph].
- [123] J. H. Chang, R. Essig, and S. D. McDermott, *JHEP* **09**, 051 (2018), [arXiv:1803.00993](https://arxiv.org/abs/1803.00993) [hep-ph].
- [124] P. Foldenauer, *Phys. Rev. D* **99**, 035007 (2019), [arXiv:1808.03647](https://arxiv.org/abs/1808.03647) [hep-ph].
- [125] M. Blennow, E. Fernandez-Martinez, A. Olivares-Del Campo, S. Pascoli, S. Rosauero-Alcaraz, and A. V. Titov, *Eur. Phys. J. C* **79**, 555 (2019), [arXiv:1903.00006](https://arxiv.org/abs/1903.00006) [hep-ph].
- [126] M. Escudero, D. Hooper, G. Krnjaic, and M. Pierre, *JHEP* **03**, 071 (2019), [arXiv:1901.02010](https://arxiv.org/abs/1901.02010) [hep-ph].
- [127] D. Croon, G. Elor, R. K. Leane, and S. D. McDermott, *JHEP* **01**, 107 (2021), [arXiv:2006.13942](https://arxiv.org/abs/2006.13942) [hep-ph].
- [128] G.-L. Lin and Y.-H. Lin, *Phys. Rev. D* **104**, 063021 (2021), [arXiv:2102.11151](https://arxiv.org/abs/2102.11151) [hep-ph].
- [129] R. L. Workman *et al.* (Particle Data Group), *PTEP* **2022**, 083C01 (2022).
- [130] T. T. Q. Nguyen, T. Linden, P. Carezza, and A. Widmark, (2025), [arXiv:2501.14864](https://arxiv.org/abs/2501.14864) [astro-ph.HE].
- [131] J. F. Navarro, C. S. Frenk, and S. D. M. White, *Astrophys. J.* **462**, 563 (1996), [arXiv:astro-ph/9508025](https://arxiv.org/abs/astro-ph/9508025).
- [132] J. F. Navarro, C. S. Frenk, and S. D. M. White, *Astrophys. J.* **490**, 493 (1997), [arXiv:astro-ph/9611107](https://arxiv.org/abs/astro-ph/9611107).
- [133] H. Duan, G. M. Fuller, J. Carlson, and Y.-Z. Qian, *Phys. Rev. D* **74**, 105014 (2006), [arXiv:astro-ph/0606616](https://arxiv.org/abs/astro-ph/0606616).
- [134] <http://snrcat.physics.umanitoba.ca/>.

Appendix A: Derivation of approximated t_{van}

In this Appendix we provide detailed derivation for the approximated formula of t_{van} [Eq. (19) in the main text] in the relativistic ($m_\chi/T_\chi \ll 1$) and the nonrelativistic ($m_\chi/T_\chi \gg 1$) limit.

1. $m_\chi/T_\chi \ll 1$

Setting $x = m_\chi/T_\chi \ll 1$ and $c = 1$ for simplicity and keeping all terms up to the leading order of $\mathcal{O}(x)$, one can approximate the BDM velocity $v_\chi \approx 1$ and the maximal scattering angle

$$\psi_{\max} \approx \cos^{-1} \left(\frac{1}{\sqrt{1+2x}} \right) \approx \sqrt{2x}.$$

Rewriting Eq. (17) in the main text as

$$\tan \theta^* = \frac{v_\chi - \cos \psi_{\max}}{\sin \psi_{\max}},$$

and use

$$\cos \psi_{\max} \approx 1 - x,$$

One gets

$$\tan \theta^* \approx \frac{x}{\sqrt{2x}} = \sqrt{\frac{x}{2}} \rightarrow \theta^* \approx \sqrt{\frac{x}{2}} \quad (\text{A1})$$

for $x \ll 1$. Rewriting Eq. (16) in the main text as

$$t_{\text{van}} = R_s \frac{\sin \theta^*}{\sin \psi_{\max}} + \frac{R_s \sin(\psi_{\max} - \theta^*)}{v_\chi \sin \psi_{\max}} - t_\nu, \quad (\text{A2})$$

and approximating the first term by

$$\frac{\sin \theta^*}{\sin \psi_{\max}} = \frac{\sin \sqrt{x/2}}{\sin \sqrt{2x}} \approx \frac{1}{2} + \frac{x}{8}$$

as well as the second term by

$$\frac{\sin(\psi_{\max} - \theta^*)}{\sin \psi_{\max}} \approx \frac{1}{2} + \frac{x}{8},$$

Eq. (A2) reduces to

$$t_{\text{van}} \approx R_s \left(\frac{1}{2} + \frac{x}{8} + \frac{1}{2} + \frac{x}{8} - 1 \right) = \frac{xR_s}{4}. \quad (\text{A3})$$

Restoring c leads to Eq. (16) for $x \ll 1$ in the main text.

2. $m_\chi/T_\chi \gg 1$

For $x \gg 1$, we expand v_χ and ψ_{\max} and keep all terms up to $\mathcal{O}(1/\sqrt{x})$. This gives $v_\chi \approx \sqrt{2/x}$ and

$$\psi_{\max} \approx \cos^{-1} \left(\frac{1}{\sqrt{2x}} \right) \approx \frac{\pi}{2} - \frac{1}{\sqrt{2x}}.$$

Taking these expressions, Eq. (17) in the main text becomes

$$\tan \theta^* = \frac{v_\chi - \cos \psi_{\max}}{\sin \psi_{\max}} \approx \frac{1}{\sqrt{2x}} \rightarrow \theta^* \approx \frac{1}{\sqrt{2x}}, \quad (\text{A4})$$

such that

$$\begin{aligned} t_{\text{van}} &= R_s \frac{\sin \theta^*}{\sin \psi_{\max}} + \frac{R_s \sin(\psi_{\max} - \theta^*)}{v_\chi \sin \psi_{\max}} - t_\nu \\ &\approx R_s \left(1 + \frac{1}{v_\chi} - 1 \right) = R_s \sqrt{\frac{x}{2}}. \end{aligned} \quad (\text{A5})$$

Once again, restoring c recovers Eq. (16) in the main text for $x \gg 1$.

We note that the peak time defined in Eq. (20) in the main text is approximately

$$t_p \approx R_s \left(\sqrt{\frac{x}{2}} - 1 \right) \approx R_s \sqrt{\frac{x}{2}}, \quad (\text{A6})$$

which is identical to Eq. (A5). Thus, t_p and t_{van} coincide under $x \gg 1$.